ACS OMEGA

http://pubs.acs.org/journal/acsodf

Article

Investigation of Cement Prepared with Microencapsulated Microorganisms

Yingying Hu, Weitao Liu, Qingtao Zhang, Xiangming Hu, and Xuelong Hu*

Cite This: *ACS Omega* 2022, 7, 2947−2959

Read Online

ACCESS | Metrics & More | Article Recommendations

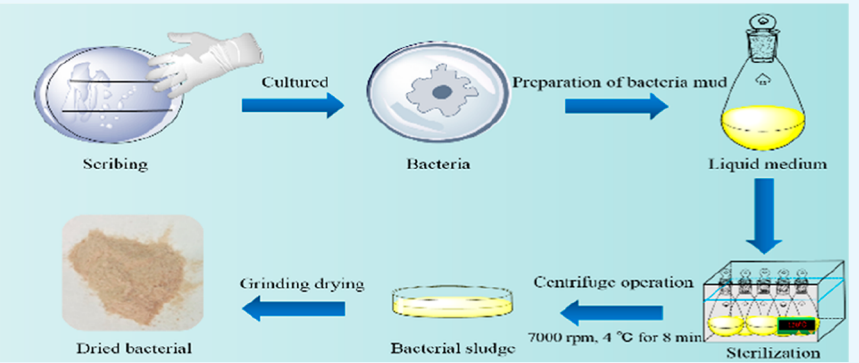

ABSTRACT: Cracks in underground rock masses cause gas leakage, seepage, and water inflow. To realize calcium carbonate deposition and mineralization filling in rock cracks, microencapsulated bacterial spores were prepared by an oil phase separation method. To optimize the microorganism growth conditions, the effects of microcapsules with various pHs, particle sizes, and amounts on microcrack self-healing were investigated through an orthogonal test, and the best conditions for repairing the cracks using microencapsulated *Bacillus sphaericus* were obtained. Infrared analysis and scanning electron microscopy were used to observe the morphological characteristics and coating performance of the microcapsules. The results showed that the microcapsules contained functional groups in the core and wall materials. The surfaces of the microcapsules prepared by the test were rough, which was beneficial for adhesion onto the fracture surface. X-ray diffraction analysis, X-ray photoelectron spectroscopy, and thermal analysis were conducted. The results showed that the microcapsules with pH = 8 and a particle size of 100 μm had the highest thermal decomposition temperature and the best thermal stability. The elements of the core and wall materials were detected in the microcapsules, and the coating had a beneficial effect. The compression and acoustic emission tests of the specimens embedding microbial capsules with different contents under different working conditions revealed that the two fractures of the specimen were due to the rupture of the microcapsule and the rupture of the rock specimen, indicating the best mechanical triggering properties and compressive properties of the microcapsule.

1. INTRODUCTION

At present, the use of in situ chemical polymerization to repair cracks is associated with chemical pollution and other issues. The microbial self-healing technology is a good solution. Pouring cement mortar takes time and labor. The operation is complex, and it is not easy to find the internal fracture of the structure. Microbial self-healing capsules are mixed with cement mortar in a certain proportion and injected into the structure. When the structure breaks under pressure, the microorganisms in the microcapsule will be activated. The spores germinate again for metabolism, induce the formation of calcium carbonate, and promote the self-healing of microcracks. After the repair, the bacterial spores are dormant again.

Wang et al.[1] used light microscopy and water permeability test results to verify that microspores can improve the self-healing efficiency of crack specimens. The results showed that the healing rate of cracks with bacterial specimens was significantly higher than that with non-bacterial specimens. The best culture conditions for the bacterial specimens were dry and wet circulation. Feng et al.[2] studied the microbially induced calcium carbonate precipitation using X-ray diffraction (XRD) analysis, which showed that the mineralized material was calcium carbonate. Compared with chemically generated

Received: October 25, 2021
Accepted: January 5, 2022
Published: January 13, 2022

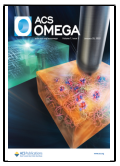

https://doi.org/10.1021/acsomega.1c05971
ACS Omega 2022, 7, 2947−2959

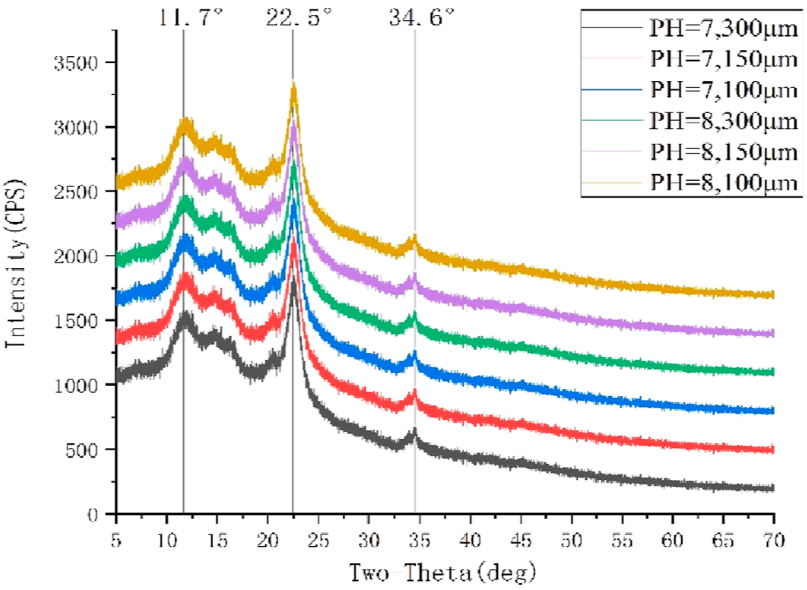

Figure 1. X-ray diffractogram of microcapsules.

calcium carbonate, the coarse calcite crystals induced by microorganisms were easier to compact, and according to the three-point bending test, self-healing concrete with a bending strength of 4.2 MPa was produced. Pungrasmi et al.[3] performed a comparative study on the microencapsulation of potential microcapsules. The study showed that when the encapsulated bacterial spores were added to concrete, problems began, such as a lack of germination inducers (nutrients, water, oxygen, etc.) and high alkalinity of mortar. These factors led to the inactivation of the encapsulated bacterial spores. Using urease produced by Pasteurella, a genus of bacilli, the University of Murdoch in Australia[4,5] compared five different concentrations of gelling solutions. The experimental results showed that 0.5 M gelling solution caused the urease-producing bacteria to maintain a maximum enzyme activity at the initial stage, thereby inducing a large amount of calcium carbonate precipitation. The results showed that the maximum uniaxial compressive strength of the specimens injected with Pasteurella mortar reached 5.7 MPa. It was found[6−11] that the microcapsules influenced the self-healing and pore structure parameters of the specimens, which influenced the deformation properties and improved the brittleness characteristics of the specimens. Other related research works[12−16] analyzed and observed the crack-healing effect before and after the addition of microbial self-repairing materials by artificially creating cracks of different widths for cement mortar specimens and found that compared with ordinary concrete, microbial concrete produced larger diameter holes, which had a certain impact on the mechanical properties of concrete. Previous studies[2,17−21] analyzed the influence of the bacterial concentration, crack size, and proportion of self-repairing carriers on the reparation of self-repairing concrete cracks through the variance analysis method of orthogonal tests. The results showed that with an increase in the bacterial concentration in the solution, the time to completely repair the crack increased first and then decreased, and the larger the crack size, the longer it took to complete the repair. The crack reparation effect was the best, when the proportion of self-healing cement-based carriers was 30%. The mineralization activity of spores after germination and the crack-healing capacity of concrete have been studied.[22−25] Some studies have focused on the optimal culture medium and the optimum external conditions for spore production.[26−29]

However, there is a problem of short survival time of microorganisms by directly repairing the damaged parts of structures with a microbial self-healing solution. Therefore, it has good prospects for application in the study and optimization of mortar prepared with microencapsulated microorganisms to repair structural damage. There is a lack of research on the mechanical triggering performance and repair performance of microcapsule-coated microorganisms. In this study, the preparation process parameters of microbial capsules were optimized. The mechanical triggering properties of microcapsules were studied by acoustic emission testing. A self-healing concrete mortar with excellent mechanical properties was prepared with *Bacillus sphaericus* as the core material and epoxy resin as the wall material, which has the engineering prospect of filling rock cracks in underground space.

2. RESULTS AND DISCUSSION

2.1. XRD Analysis of Microcapsules. When the pH was between 7 and 8, the particle sizes were 300, 150, and 100 μm, and six types of microcapsules were identified by XRD analysis. The results are presented in Figure 1. It is observed from the test results that the diffraction peaks of the microcapsules under six different conditions can correspond to each other. It is seen from the X-ray diffractogram that the radiation peak value of the microcapsule broadened and weakened at 2θ = 11.7, 22.5, and 34.6°. The phenomenon of broadening and weakening of the microcapsules was clear at 2θ = 22.5°. This may be due to the decrease in the particle size, non-uniform distribution of the composition, and the presence of microbial spores in the microcapsule, as the lack of a regular distribution weakens the diffraction intensity of the microcapsules to a certain extent. However, the outer layer of polydimethylsiloxane and epoxy resin caused the microcapsules prepared under different working conditions to have different thickness attachments, resulting in a change in the diffraction diffractogram. However, it is seen from the map that the crystal types of the self-healing microbial microcapsules under different

https://doi.org/10.1021/acsomega.1c05971
ACS Omega 2022, 7, 2947−2959

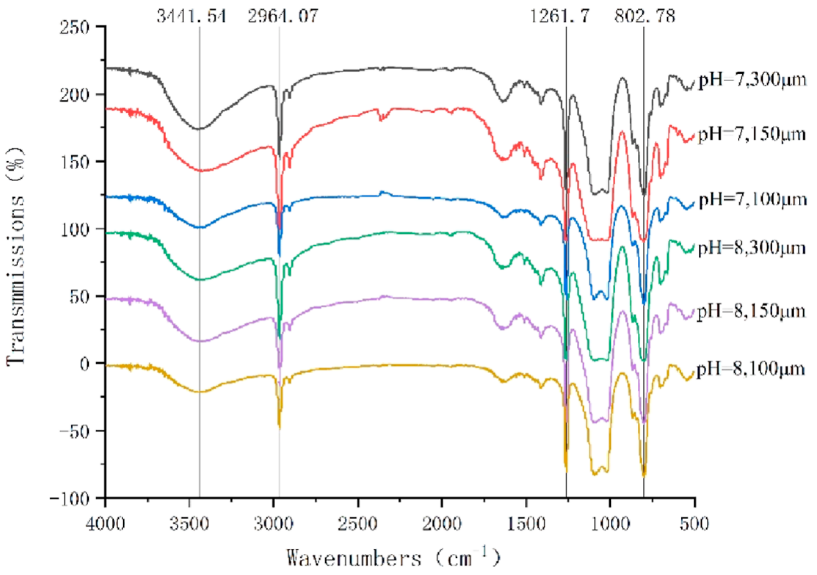

Figure 2. Infrared spectrogram of microcapsules.

working conditions are the same, indicating that the pH value and the particle size of the culture have no influence on structural damage.

2.2. Infrared Spectrum Analysis of Microcapsules. The absorption spectra of the six types of microcapsules with different pHs and particle sizes were analyzed, as shown in Figure 2. The results show that the variation in the transmittance of microcapsules with different particle sizes and pHs was almost the same, and the structure and composition of the microcapsules were the same. With a decrease in the particle size of the microcapsules, the transmittance of the sample increased. The absorption peak at 3500 cm^{-1} decreased, and the OH bond between the molecules expanded, indicating that weakly basic nutrients existed in the core. In the 810−750 cm^{-1} range, there is a strong peak reduction and in-plane CH bond bending, and there are three adjacent hydrogen atoms. The absorption peaks at 1260−1000 cm^{-1} decreased, and the C−O bond stretched and contracted. The infrared transmittance peaks of the microcapsules with different pH values and particle sizes fluctuated between 0 and 25. The peak value of 2,4,6-tris(diethylamino)phenol decreased from 1390 to 1330 cm^{-1}, and the OH bond of phenol was bent in the plane, which indicate the existence of the curing agent 2,4,6-tris-(diethylamino)phenol. The results of infrared spectroscopy showed that the microcapsules were mainly composed of microorganisms and functional groups of microcrystalline cellulose as the core material and epoxy resin (E-51 type) as the wall material. The above phenomenon may be due to the non-uniform particle size distribution, which leads to different thicknesses of the outer wall material film of the microcapsule during the stirring and coating operation of epoxy resin, resulting in the alteration of the peak value. The transmittance curve of the microcapsules with a pH value of 7 and a particle size of 300 μm in the 3441.54−3007.30 cm^{-1} range increased faster than those of the other microcapsules because of the increase in the number of substituted CH bonds of alkanes and the CH bonds of benzene. The permeability peak of microcapsules with a pH value of 7 and a particle size of 150 μm was 2359.33 cm^{-1}, which was different from that of other microcapsules. However, it was found that the encapsulation of microcapsules had good integrity through the vibration and stretching of bonds between functional groups and crystal atoms.

2.3. Scanning Electron Microscopy Analysis of Microcapsules. The encapsulated microcapsules were observed by scanning electron microscopy (SEM), as shown in Figure 3.

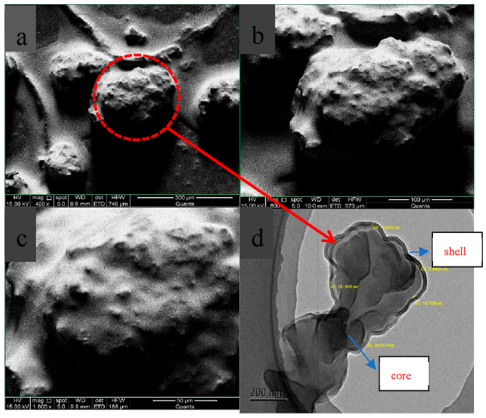

Figure 3. SEM and TEM images of microcapsules. (a) SEM image at 400× magnification; (b) SEM image at 800× magnification; (c) SEM image at 1600× magnification; and (d) TEM image.

The results showed that the coated microcapsules were irregular particles, and the surfaces of the microcapsules were rough with obvious unevenness. The test shows that microcapsules with a rough surface were conducive to the mixing of mortar and better adhesion to the surface of the rock specimen. It is observed that there was a layer of colloidal epoxy resin film on the outer wall of the microcapsule, which can prevent the bacteria from losing their activity because of the highly alkaline environment during mixing of the bacterial spores into the cement mortar and effectively protect the bacterial spores. The surface roughness of the microcapsules may be due to the uneven distribution of the bacterial spore powder in cellulose. However, the mortar was used to manually grind the core material to break the complete spherical core material and form a rough section. Moreover,

https://doi.org/10.1021/acsomega.1c05971
ACS Omega 2022, 7, 2947−2959

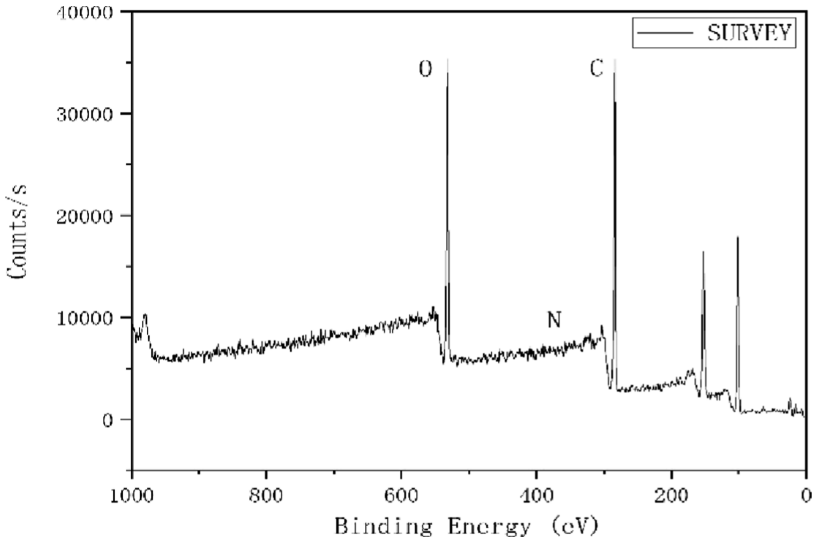

Figure 4. XPS spectrum of microcapsules.

when studying the performance of crack reparation, it was found that the concave−convex surface of the microcapsules did not have a greater impact on the repair effect. In contrast, a certain roughness increases the adhesion of the microcapsules, rock specimens, and cement mortar.

The core−shell structure of microcapsules can be observed more clearly by transmission electron microscopy (TEM) and SEM. The encapsulated microcapsules were observed by TEM, and the results are shown in Figure 3. The results showed that the surface of the microbial core material has been successfully encapsulated by the shell with fine coverage.

2.4. X-ray Photoelectron Spectroscopy Analysis of Microcapsules. The microcapsules were analyzed by X-ray photoelectron spectroscopy (XPS), as shown in Figure 4. The results show the presence of C, O, N, P, S, and other elements in the microcapsules. The peak value of C was located at 284.65 eV, and its content was approximately 68.72%. The peak value of O was located at 532 eV, and its content was approximately 30.65%. The peak value of N was located at 397.96 eV, and its content was approximately 0.41%. The molecular formula of the wall material with epoxy resin as the main material was $(C_{11}H_{12}O_3)_n$. Only C, H, and O were present in the epoxy resin, while the elements in microorganisms mainly included C, H, O, N, P, and S. Therefore, as per the XPS test results, N and trace P and S existed in the core material. The contents of C and O were the sum of the two elements of the core material and epoxy resin. However, a small amount of urea, sodium chloride, soybean peptone, casein peptone, and hydroxypropyl methylcellulose were added to the microcapsule core material as nutrient substances of bacterial spores, which contained small amounts of P and S. Moreover, to complete the coating, polydimethylsiloxane added still had a small amount of adhesion on the surface of the microcapsules, and the trace elements in the polydimethylsiloxane were detected by XPS. The presence of these elements indicates that the microcapsules had good coating properties.

2.5. Particle Size Analysis of Microcapsules. By analyzing the size of microcapsules prepared under different conditions, as shown in Figures 5−7, along with the analysis of the morphological characteristics of the microcapsules and XPS data, it was estimated that the particle sizes of the three

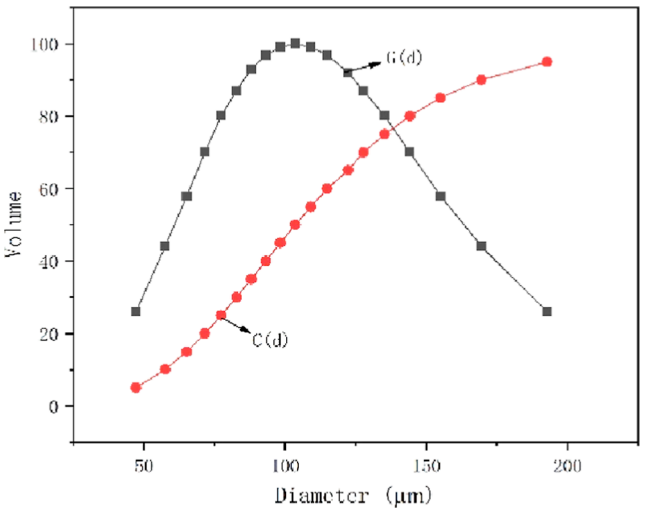

Figure 5. Particle size diagram of the microcapsule with a particle size of 100 μm.

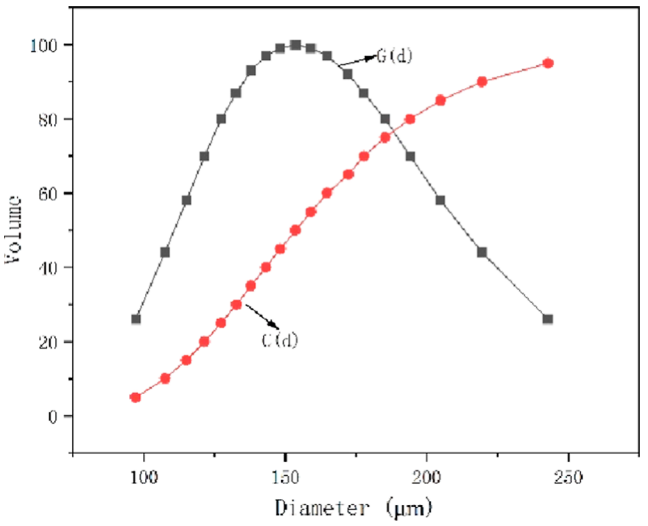

Figure 6. Particle size diagram of the microcapsule with a particle size of 150 μm.

https://doi.org/10.1021/acsomega.1c05971
ACS Omega 2022, 7, 2947−2959

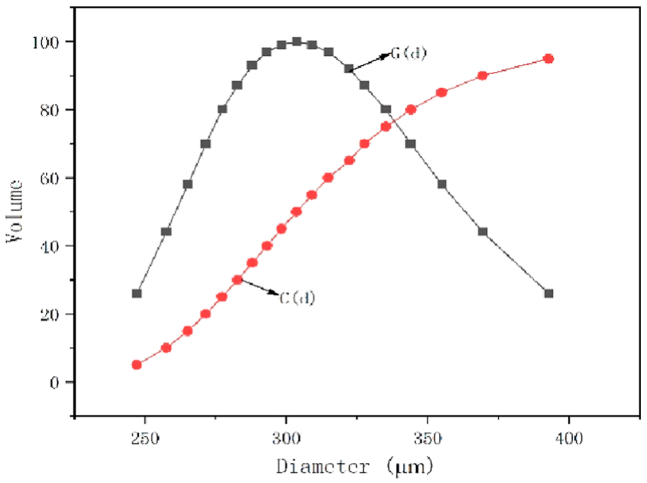

Figure 7. Particle size diagram of the microcapsule with a particle size of 300 μm.

working conditions were approximately 100, 150, and 300 μm. The G (d) curve represents the differential distribution and the relative distribution of different microcapsule particle sizes. The C (d) curve represents the integral distribution and the cumulative distribution of different microcapsule particle sizes. Figure 5 shows that the particle size distribution range of microcapsule samples with a median particle size of 100 μm is more concentrated and uniform, Figure 6 shows that the median particle size of microcapsule samples is more concentrated in the range of 150 μm, and Figure 7 shows that the particle size distribution range of microcapsule samples with a median particle size of 300 μm is more concentrated and uniformly even. Microcapsule core materials with different particle sizes were prepared using a planetary ball mill with grinding times of 2, 4, and 5 h. It was found that the distribution of microcapsules with the same particle size was uneven by electron microscopy. The reason for this phenomenon may be the uneven grinding force and angle when using an electric ball mill. Microcapsules with different granularities affected the distribution of the cement mortar. When the grains were too small, the bacterial content in the cellulose was low, and only a small amount of calcium carbonate precipitation was produced in the fissure area, which cannot achieve a good repair effect. When the particle size of the microcapsules was too large, when the mortar was mixed with cement mortar, the proportion of mortar was small, and the proportion of microcapsules was large, which affected the compressive strength of the structure to some extent.

2.6. Thermal Stability Analysis of Microcapsules. Thermogravimetry (TG) and differential TG (DTG) analyses were performed on the microcapsules. The results are shown in Figures 8 and 9, respectively. The initial reaction temperature of microcapsules with a pH value of 7 and a particle size of 300 μm was 164.49 °C, the final reaction temperature was 616.01 °C, and the residual amount was 14.207%. The initial reaction temperature of the microcapsules with a pH value of 7 and a particle size of 150 μm was 205.37 °C, the final reaction temperature was 609.82 °C, and the residual amount of reaction was 16.83%. The initial temperature of the microcapsules with a pH value of 7 and a particle size of 100 μm was 192.88 °C, the final temperature was 610.80 °C, and the remaining amount was 17.471%. The initial temperature of the microcapsules with a pH value of 8 and a particle size of 300

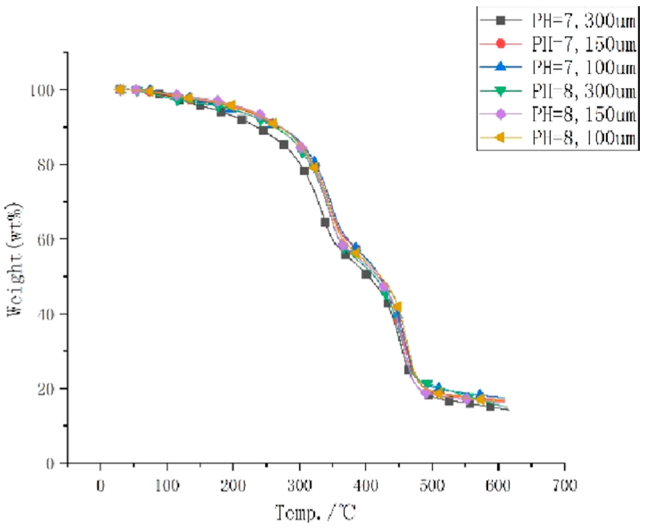

Figure 8. TG curve of microcapsules.

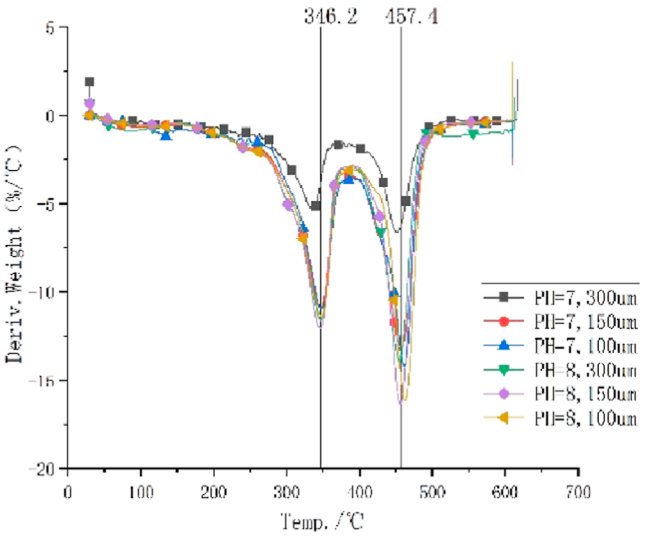

Figure 9. DTG curve of microcapsules.

μm was 192.54 °C, the final temperature was 612.80 °C, and the remaining amount was 14.993%. The initial reaction temperature of the microcapsules with a pH value of 8 and a particle size of 150 μm was 216.44 °C, the final reaction temperature was 609.68 °C, and the residual amount was 16.137%. The initial temperature of the microcapsules with a pH value of 8 and a particle size of 100 μm was 210.72 °C, the final temperature was 610.28 °C, and the residual amount was 16.417%. The thermal decomposition stability of the microcapsules under the other five reaction conditions was significantly better than that of the microcapsules with pH = 7 and a particle size of 300 μm. The microcapsules' outer wall containing polydimethylsiloxane and epoxy resins may adhere to a small amount of moisture, resulting in a slow decline in the platform area.

In DTG curves, two mass losses were observed, and the first one occurred at 346.2 °C, corresponding to a water loss process. The second loss occurred at 457.4 °C, corresponding to the loss of CO_2. Owing to the large particle size of 300 μm, the decomposition rate was slow. The reaction was incomplete, and the amount of the residual reaction was large.

https://doi.org/10.1021/acsomega.1c05971
ACS Omega 2022, 7, 2947−2959

2.7. Microcapsule Repair Performance Analysis. Uniaxial compression tests and acoustic emission tests were performed on the specimens cured for 14 days. The experimental process is illustrated in Figure 10.

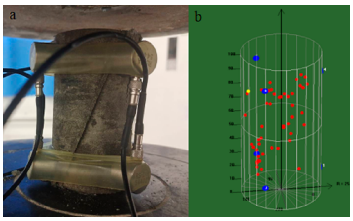

Figure 10. Experimental process. (a) Specimen failure diagram and acoustic emission location and (b) 3D energy locus diagram of the specimen.

2.7.1. Mechanical Test Analysis. Uniaxial compression tests were carried out on specimens with different pHs, microcapsule sizes, and microcapsule contents on an orthogonal experimental table. The stress−strain curve for each specimen is shown in Figure 11. When the pH value was 7, the content of microcapsules was 2%, and the particle size was 300 μm, the final failure occurred at 7.3 MPa. Before the final failure, two deformations occurred, one at 2.1 and another at 7 MPa. When the pH value was 7, the microcapsule content was 4%, and the particle size was 150 μm, the final failure occurred at 6.6 MPa. Deformation occurs before the final failure, and the stress was 0.9 MPa. When the pH value was 7, the content of the microcapsules was 6%, and the particle size was 100 μm, the specimen was finally destroyed at 12.5 MPa. Before the final destruction, there was a deformation, and the stress was 0.9 MPa. When the pH value was 8, the content of microcapsules was 2%, and the particle size was 100 μm, the specimen was destroyed at 12.3 MPa, and there was no deformation before the final destruction. When the pH value was 8, the microcapsule content was 4%, and the particle size was 300 μm, the final failure occurred at 9.8 MPa. Before the final failure, deformation occurred, and the stress was 1.4 MPa. When the pH value was 8, the content of microcapsules was 6%, and the particle size was 150 μm, the final failure occurred at 9.7 MPa, and the final failure occurred at 1 MPa. When the pH value was 9, the content of microcapsules was 2%, and the particle size was 150 μm, the specimen was finally destroyed at 18.8 MPa. Before the final destruction, deformation occurred, and the stress was 1.1 MPa. When the pH value was 9, the microcapsule content was 4%, and the particle size was 100 μm, the final failure occurred at 15.2 MPa. Before the final failure, deformation occurred, and the stress was 1.5 MPa. The cause of multiple deformations may be the rupture of microcapsules and cement mortar in cracks, and the final deformation was caused by the failure of the rock specimens. The average stress of microcapsules and mortar mixture in cracking was 1.27 MPa, and the ultimate stress of specimen was 11.52 MPa. When the pH value was 9, the microcapsule content was 2%, and the particle size was 150 μm, the failure stress and strength were the highest.

Based on the previous literature on the mechanical test of rock specimens,[30−33] the complete stress−strain curve was measured for the tested specimens, and they showed good elastic−plastic properties before the peak value. The shape of the stress−strain curve was similar to that of the standard rock, but the falling section was steeper than that of the standard rock specimen, and the stress decreased faster, indicating that the ductility of the rock specimen filled with microcapsules was decreased but maintained a high strength. It was found that the compressive strength of rock specimens filled with microbial capsules in this experiment reached 6.6−18.8 MPa, which realized a higher degree of strength repair compared with the original compressive strength of shale (11.5−22.8 MPa). Before the final failure, all the tested pieces experienced the first deformation, which was the stress peak caused by the rupture of microcapsules, indicating that the prepared microbial capsules have excellent mechanical triggering properties.

2.7.2. Acoustic Emission Testing. Acoustic emission testing was conducted on the cured specimens, as shown in Figure 12. It can be seen that the energy and the impact count of the pH = 7 microcapsules are higher, and the energy and the impact count of the microcapsules with pH = 9 were at a relatively low level. The impact count of microcapsules with pH = 7 with 2% addition and 300 μm particle size are relatively uniform throughout the whole time. When the values of pH were 7 and 8, the amount of microcapsules was 2%, and the particle size was 100 μm, the impact count appeared at the beginning and at the fracture of the specimen; when the pH value was 9, the content of microcapsules was 4%, and the particle size was 100 μm, the peak of the impact count appeared in the first half. The peak values of the energy and impact count were earlier than those of the other working conditions. Combined with the impact count tests, it can be seen that the location map of the specimens under different working conditions may roughly correspond to the failure of the specimens. The location points of the pH = 8 and pH = 9 specimens were sparse compared with the specimens at pH = 7, indicating that there are many times of strength relaxation damage in the failure surface of the specimen. From the energy curve, it can be seen that the specimens with pH = 7 acid and alkali perfusion showed uneven peaks before and after the failure of the specimen, indicating more energy loss during the crushing process. However, the energy of the pH = 8 and pH = 9 specimens before and after cracking was relatively smooth, and a larger amount of energy was released at the moment of failure. The destruction of the specimen was impacted by block fracture, and the strength of the specimen with larger alkaline microcapsules was slightly higher.

2.8. Influence of the Microcapsule Content on Cement Mortar. *2.8.1. Effect on the Fluidity of Cement Mortar.* Table 1 shows the influence of microcapsule content on the fluidity of cement mortar. Analysis of the experimental results showed that the fluidity of mortar decreased with the increase of the microcapsule content. Because bacteria were added to cement mortar, the negative charge of the bacterial cell body and its secretion may adsorb cement particles, making it difficult for cement particles to move with each other, to reduce the fluidity of cement mortar.

2.8.2. Influence on the Setting Time of Cement Mortar. The increase of the microcapsule content will have a certain impact on the performance of cement-based materials, reduce its fluidity, delay the setting time of cement mortar, and then cause the loss of cement mortar strength. However, controlling the content of microcapsules within an appropriate range (accounting for less than 4% of cementitious materials) will not have a significant impact on cement-based materials, as shown in Table 2.

https://doi.org/10.1021/acsomega.1c05971
ACS Omega 2022, 7, 2947−2959

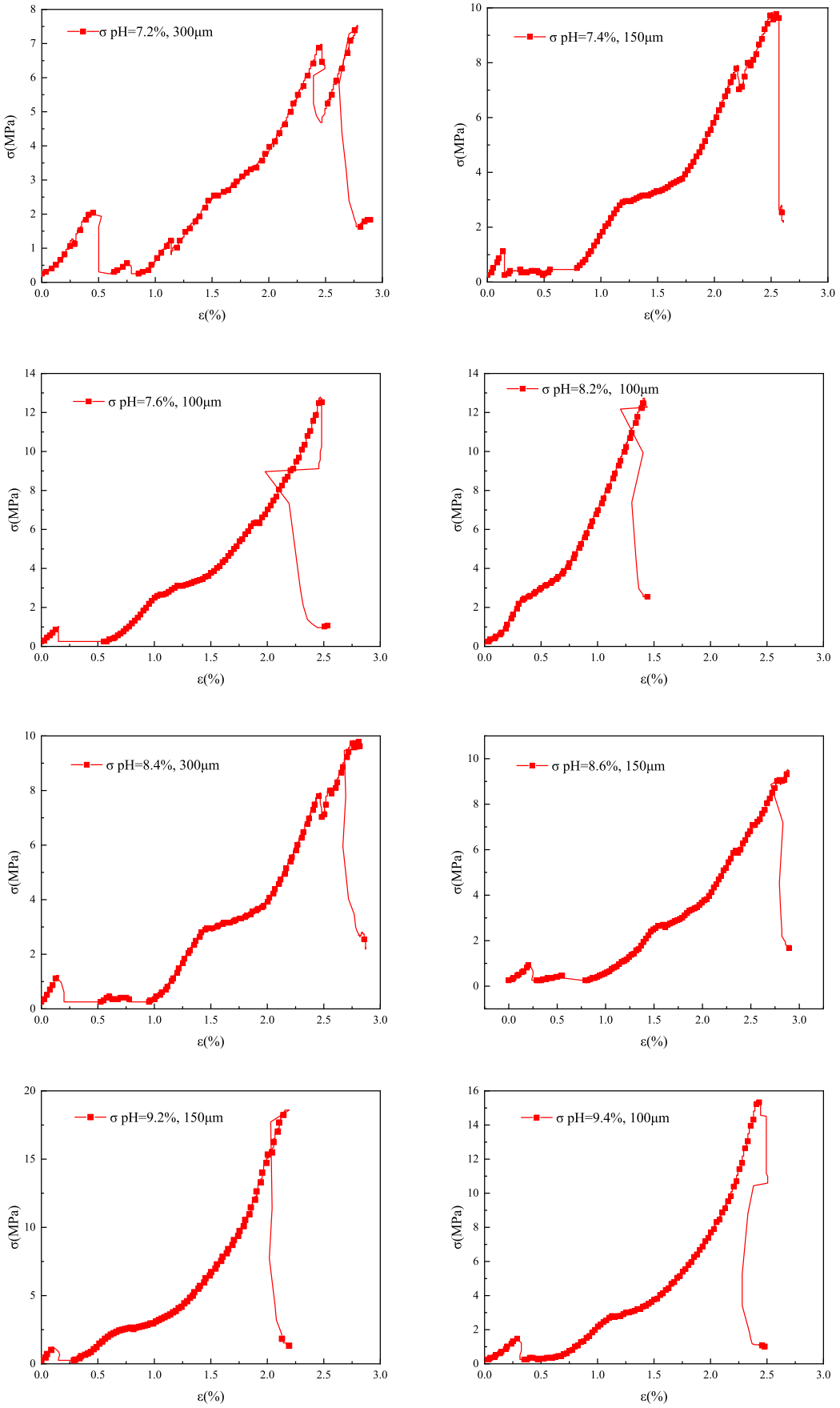

Figure 11. Stress−strain curve of specimens.

https://doi.org/10.1021/acsomega.1c05971
ACS Omega 2022, 7, 2947−2959

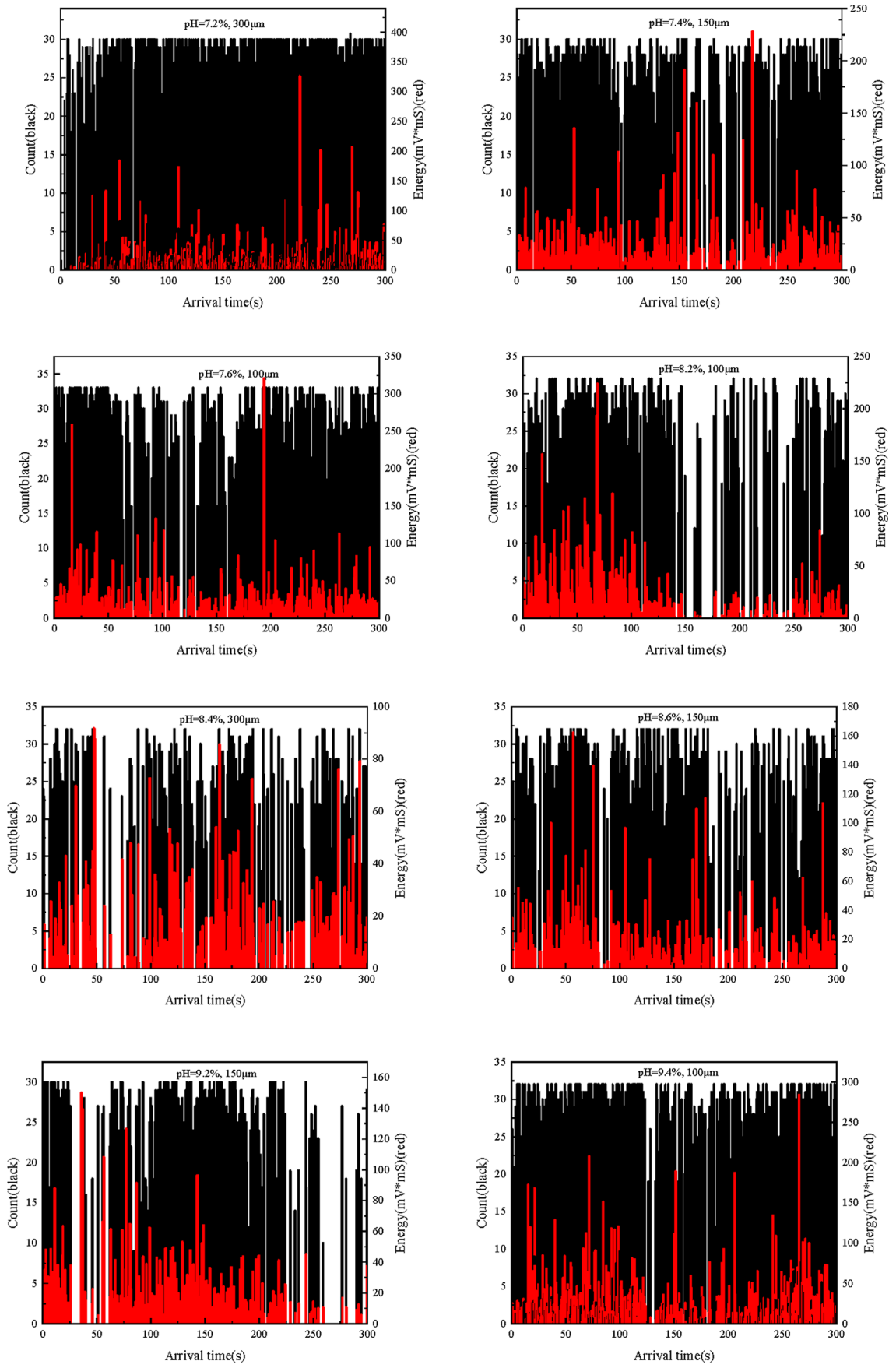

Figure 12. Energy and count curve of specimens.

https://doi.org/10.1021/acsomega.1c05971
ACS Omega 2022, 7, 2947−2959

Table 1. Fluidity of Mortar with Different Microcapsule Contents

group	cement/g	sand/g	water/g	microcapsule/g	sinking depth/cm
1	270	810	270	0	5.5
2	270	810	270	5.4	5.3
3	270	810	270	10.8	5.0
4	270	810	270	16.2	4.8

3. CONCLUSIONS

Through an experimental study on the preparation of mortar with microencapsulated microorganisms, the following conclusions were obtained.

(1) Fourier transform infrared (FTIR) analysis showed that the infrared spectra of microbial capsules with different pHs and particle sizes were basically the same, and the functional groups containing the core material and the wall material had better encapsulation.
(2) SEM was used to observe the morphology of the microcapsules. It was found that the surface of the microcapsules was concave−convex and rough, which was conducive to the mixing of the microcapsules and cement mortar and better attachment to the fracture surface.
(3) Through XRD and XPS, it was found that the pH and the particle size did not damage the structure of the microcapsules, the elements of the core and wall materials were detected in the microcapsules, and the coating effect was good.
(4) The results showed that the particle sizes of the three types of microcapsules with different grinding times were 100, 150 and 300 μm, respectively. The microcapsule with 150 μm particle size contained an appropriate number of bacterial spores and had the least influence on the strength of the specimen.
(5) The results showed that the microcapsule with pH = 8 and a particle size of 100 μm had the highest thermal decomposition temperature and the best thermal stability.
(6) The compressive and acoustic emission tests of the specimens under different working conditions revealed that the specimens were damaged twice. The first was owing to the rupture of the microcapsule, and the second was owing to the rupture of the rock specimen, which indicated that the prepared microcapsules had good mechanical triggering performance. The strength of the samples with pH = 8 and pH = 9 microcapsules was greater than that with pH = 7 microcapsules.

4. EXPERIMENTAL SECTION

4.1. Preparation of Bacterial Mud. The experimental drugs used in this experiment are shown in Table 3.

Distilled water or nutrient solution (0.3 mL) was obtained using a sterilized rubber-head dropper. Then, it was added to a freeze-drying tube and gently shaken until it completely dissolved; this was done on the sterile workbench. The dissolved suspension was dropped into a two-tube slant solid medium or Lysogeny broth (LB) liquid medium and activated in a biochemical incubator (30 °C, 18−24 h). As shown in Figure 13, extended culture of *B. sphaericus* was performed in LB and agar solid medium using the scribing method in a sterile operating platform.

As shown in Figure 14, the liquid medium was prepared using LB broth medium, anhydrous calcium chloride, and urea, and the pH value of the bacterial solution was adjusted with sodium hydroxide solution. The prepared bacterial solution was sterilized in a high-pressure and high-temperature sterilization pot (120 °C, 20 min). After cooling the liquid, it was inoculated with an inoculation ring, with 1:100 bacteria, and placed in a vibration incubator (28 °C, 72 h).

Centrifugation was carried out (7000 rpm, 4 °C for 8 min). After centrifugation, the upper layer of the supernatant was poured into a waste liquid tank, the sediment in the centrifuge tube was removed and dried in a drying instrument (72 h, room temperature) and then ground to obtain the bacterial spore powder (represented in Figure 15).

4.2. Preparation of Microcapsules. Bacterial spores as a core material were coated with shells to form microcapsules. To ensure the long-term survival of the microbial spores in a highly alkaline environment, a waterproof epoxy resin was used to coat the spore core material to form a protective film.

The spore suspension was stirred and mixed to paste. Microcrystalline cellulose was added as an auxiliary reagent for core material volume expansion. Hydroxypropyl methylcellulose was added to increase the adhesion between cellulose and spores, and appropriate amounts of urea, soybean peptone, casein peptone, sodium chloride, and so forth were mixed in water to provide high-quality survival nutrients for spore survival and stirred until the spores agglomerated. The core material was screened with a 0.335 mm sieve and dried in a blast drying oven at 40 °C. Subsequently, the dried core material was ground to different particle sizes by a planetary ball mill, as shown in Figure 16.

According to the core wall ratio of 1:3, E-51 epoxy resin and spore core material particles were weighed, and the two were mixed evenly in a beaker. The two particles were heated in a water bath (50 °C, 5 min). According to the ratio of epoxy resin to 2,4,6-tris-(dimethylaminomethyl)phenol (10:1), a 2,4,6-phenol curing agent was added for 30 min of water bath pre curing. Then, polydimethylsiloxane was added at the concentration of 50 g, and the rotating speed was set to 300 rpm for 1 h. After completion of the reaction, the mixture was filtered and washed with absolute ethanol, and microcapsules were obtained after drying, as shown in Figure 17.

4.3. Preparation and Injection of the Microcapsule-Coated Microbial Mortar. The dried microcapsules were designed for orthogonal tests according to various pH levels, contents, and particle size of the microcapsules and added to

Table 2. Setting Time of Cement Mortar with Different Microcapsule Contents

group	cement/g	sand/g	water/g	microcapsule/g	initial setting time	final setting time
1	270	810	270	0	1 h 21 min	4 h 16 min
2	270	810	270	5.4	2 h 13 min	5 h 27 min
3	270	810	270	10.8	3 h 32 min	5 h 46 min
4	270	810	270	16.2	3 h 48 min	6 h 11 min

https://doi.org/10.1021/acsomega.1c05971
ACS Omega 2022, 7, 2947−2959

Table 3. Experimental Drugs

raw material	purity	manufacturer
E-51 epoxy resin	industrial grade	Suzhou Colorful Stone Composite
2,4,6-tris(dimethylaminomethyl)phenol	industrial grade	Shanghai Aladdin Reagent
polydimethylsiloxane	industrial grade	Guangzhou Xumei Chemical Technology
absolute ethanol	analytically pure	Tianjin Damao Chemical Reagent
casein peptone	analytically pure	Beijing Bai Ao Lai Bo Science and Technology
soybean peptone	analytically pure	Beijing Bai Ao Lai Bo Science and Technology
sodium chloride	industrial grade	Wuxi Yatai United Chemical Co., Ltd
urea	analytically pure	Beijing Bai Ao Lai Bo Science and Technology
hydroxypropyl methyl cellulose	industrial grade	Beijing Bai Ao Lai Bo Science and Technology
microcrystalline cellulose	analytically pure	Beijing Bai Ao Lai Bo Science and Technology
B. sphaericus		Guangdong Microbial Strain Collection Center
distilled water		laboratory instrument self-made
agar		Beijing Bai Ao Lai Bo Science and Technology
anhydrous calcium chloride		Binzhou Anlida Chemical Co., Ltd
LB broth medium		Beijing Bai Ao Lai Bo Science and Technology

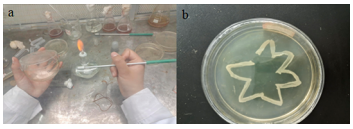

Figure 13. Extended culture of *B. sphaericus*. (a) Extended culture of bacteria by scribing and (b) bacteria after culture.

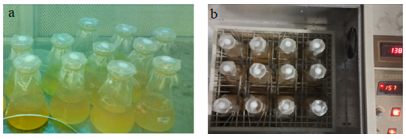

Figure 14. Preparation and culture of bacteria liquid. (a) Liquid medium awaiting cooling after sterilization and (b) bacterial solution in shaking culture.

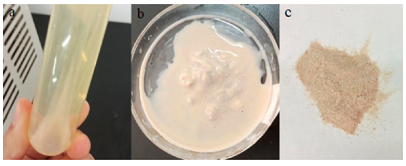

Figure 15. Preparation of bacteria mud. (a) Centrifuged broth; (b) bacterial sludge; and (c) dried bacterial spore powder after grinding.

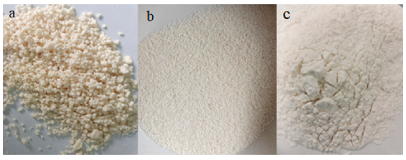

Figure 16. Preparation of the core material. (a) Core material after screening; (b) dried core; and (c) core material after grinding.

Figure 17. Microcapsules.

the precut rock cracks, as shown in Figure 18. Follow-up tests were carried out by curing with nutrient solution.

Figure 18. Specimen preparation. (a) Mixing microcapsules with a cement mortar; (b) application of a mixed mortar; (c) rock specimen injected with a microencapsulated mortar; and (d) maintenance process.

4.4. Experimental Design. The effects of these variables on the crack repair performance of microcapsules were explored by adjusting the dosage of microcapsules in the mortar, the pH value, and the particle size of microcapsules. The specific scheme design is presented in Table 4.

Table 4. Experimental Design

no.	pH of core material	microcapsule dosage (%)	pre-pressure (%) (σ_{max})	particle size (μm)
1	7	2	40	300
2	7	4	60	150
3	7	6	80	100
4	8	2	60	100
5	8	4	80	300
6	8	6	40	150
7	9	2	80	150
8	9	4	40	100
9	9	6	60	300

4.5. Performance Test of Microcapsules. *4.5.1. Investigation of Microcapsules Using XRD Analysis.* The microbial microcapsules were ground into powder to obtain samples for testing. In the XRD analyzer, the distribution of atoms in the material was analyzed using varying spatial distribution directions and intensities of the diffraction rays projected onto the material.

https://doi.org/10.1021/acsomega.1c05971
ACS Omega 2022, 7, 2947−2959

4.5.2. Investigation of Microcapsules Using SEM. The microcapsule samples were fixed on a metal test bench with a conductive adhesive for testing. They were sprayed under vacuum with gold atoms for 20 s, and the emission voltage was used to observe the samples.

4.5.3. Infrared Spectrometry Analysis of Microcapsules. The dry finished microcapsules and the auxiliary agent (KBr) were evenly mixed in a mortar at a ratio of 1:100, and a spoonful of mixed powder was obtained. A 5 mm-diameter sheet was made by manual pressing in laboratory. The absorbance and transmittance of the microcapsules were measured by FTIR spectroscopy.

4.5.4. Investigation of Microcapsules by XPS. The oil on the surface of the microcapsule was first cleaned with cyclohexane and then with anhydrous ethanol. A small amount of vacuum-dried microcapsule samples were attached to the double-sided adhesive tape and fixed on a photoelectron spectroscopy table for testing.

4.8.5. Investigation of the Thermal Stability of Microcapsules. 0.5 ± 0.1 mg of microcapsule sample was taken, and the nitrogen flow rate was set to 20 mL/min. The programed temperature technology was used to determine the relationship between the power difference of the given and reference substances and the temperature, as well as the relationship between the mass and the temperature in the reaction process.

4.5.6. Microcapsule Repair Performance Test. An electric servo uniaxial universal pressure testing machine and a DS-2 acoustic emission tester were used to measure and analyze the compressive properties of the specimens and the distribution of microcapsules in the mortar, respectively.

4.6. Test on the Influence of Microcapsules on the Properties of Cement Mortar. *4.6.1. Fluidity Test of Cement Mortar.* The SC-145 mortar consistency tester was used in the experiment, and the mortar was prepared at a certain ratio according to Table 5 adding unequal quantity of microcapsules and stirring evenly. Before the start of the experiment, a layer of lubricating oil on the pole of the cone was rubbed and the screws were released to let it slide freely. The inner wall and the cone of the wet container were wiped with a wet cloth. The stirred mortar was put into the conical container, and the mortar depth was lower than the edge 10 mm. The tamping bar was inserted 25 times from the center to the edge and knocking the edge of the container. The cross arm was lifted to the proper position by raising the scale, so that the tip of the cone contacted the surface of the mortar mixture on the surface of the container. When the scale was loosened, the stopwatch was timed, and the screws were screwed. The standard vertebra was sunk into the mortar mixture with its own weight, and the screw was screwed to the depth after 10 s, as shown in Figure 19.

Table 5. Materials Ratio

group	cement/g	sand/g	water/g	microcapsule ratio/%	microcapsule content/g
1	270	810	270	0	0
2	270	810	270	2	5.4
3	270	810	270	4	10.8
4	270	810	270	6	16.2

4.6.2. Cement Mortar Setting Time Testing. According to the standard requirements, the initial setting time of ordinary Portland cement cannot be less than 45 min, and the final setting time cannot exceed 10 h at the latest. In engineering applications, the setting time of cement mortar has a very important influence on the construction method and the progress of the project. Therefore, it is necessary to carry out tests to find out the influence of the amount of self-healing microcapsules on the setting time of cement mortar to determine whether it meets the requirements of construction. Four groups were set in the experiment, and the specific matching ratio of each group is shown in Table 5.

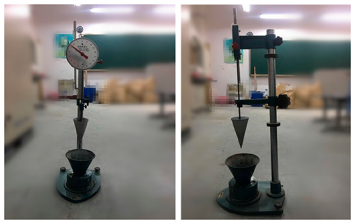

Figure 19. Mortar consistency meter.

A ZSK-100 mortar setting time tester was used for the test. The cement mortar was prepared according to a certain proportion, mixed evenly, and put into the test mold. It was smoothed from 10 mm at the top of the container. If there was no water on the surface of the mortar, it would not be removed. The test mold was placed on the disc. The pressure indicator should be cleared at this time. Then, the pressure was pressed vertically down the handle by hand, and the needle was vertically and evenly penetrated the sand loading of 25 mL in 10 s. At this time, the pressure indicator displayed the first measurement value and the position nut was then adjusted to the appropriate position. The pressure bar was loosened, and the test needle was reset under the spring force. This step was repeated every half an hour. When the resistance value of 0.3 MPa was reached, it was measured every 15 min, and when the resistance value of 0.7 MPa was reached the measurement was stopped, as shown in Figure 20.

Figure 20. Mortar setting time tester.

DATA AVAILABILITY STATEMENT

All data, models, and code generated or used during the study are available in the article.

AUTHOR INFORMATION

Corresponding Author

Xuelong Hu − *Key Laboratory of Safety and High-Efficiency Coal Mining, Ministry of Education, Anhui University of Science and Technology, Huainan 232001, China;* orcid.org/0000-0003-1783-0935; Email: xuelonghu@aust.edu.cn

https://doi.org/10.1021/acsomega.1c05971
ACS Omega 2022, 7, 2947−2959

Authors

Yingying Hu − *Department of Chemical Engineering and Safety, Bin Zhou University, Bin Zhou 256600, China; Key Laboratory of Safety and High-Efficiency Coal Mining, Ministry of Education, Anhui University of Science and Technology, Huainan 232001, China; College of Safety and Environmental Engineering, Shandong University of Science and Technology, Qingdao 266590, China*

Weitao Liu − *College of Safety and Environmental Engineering, Shandong University of Science and Technology, Qingdao 266590, China*

Qingtao Zhang − *Department of Architectural Engineering, Bin Zhou University, Bin Zhou 256600, China;* orcid.org/0000-0002-6972-8265

Xiangming Hu − *College of Safety and Environmental Engineering, Shandong University of Science and Technology, Qingdao 266590, China*

Complete contact information is available at: https://pubs.acs.org/10.1021/acsomega.1c05971

Notes

The authors declare no competing financial interest.

■ ACKNOWLEDGMENTS

This work was funded by the National Natural Science Foundation of China (grant no. 51904032), the National Natural Science Foundation of China (grant no. 51874192), Open research fund of Key Laboratory of Ministry of Education jointly constructed by the Ministry of Education of the People's Republic of China for safe and efficient mining of coal mines (JYBSYS2020205), and Scientific Research Foundation of Binzhou University (grant no. BZXYLG1914).

■ REFERENCES

(1) Wang, J. Y.; Soens, H.; Verstraete, W.; De Belie, N. Self-healing concrete by use of microencapsulated bacterial spores. *Cem. Concr. Res.* **2014**, *56*, 139−152.

(2) Feng, J.; Chen, B.; Sun, W.; Wang, Y. Microbial induced calcium carbonate precipitation study using Bacillus subtilis with application to self-healing concrete preparation and characterization. *Constr. Build. Mater.* **2021**, *280*, 122460.

(3) Pungrasmi, W.; Intarasoontron, J.; Jongvivatsakul, P.; Likitlersuang, S. Evaluation of Microencapsulation Techniques for MICP Bacterial Spores Applied in Self-Healing Concrete. *Sci. Rep.* **2019**, *9*, 12484.

(4) Liang, C.; Cord-Ruwisch, R. Selective enrichment and production of highly urease active bacteria by non-sterile (open) chemostat culture. *J. Ind. Microbiol. Biotechnol.* **2013**, *40*, 1095−1104.

(5) Mondal, S.; Das, P.; Datta, P.; Ghosh, A. Deinococcus radiodurans: A novel bacterium for crack remediation of concrete with special applicability to low-temperature conditions. *Cem. Concr. Compos.* **2020**, *108*, 103523.

(6) Wu, M.; Hu, X.; Zhang, Q.; Cheng, W.; Xue, D.; Zhao, Y. Application of bacterial spores coated by a green inorganic cementitious material for the self-healing of concrete cracks. *Cem. Concr. Compos.* **2020**, *113*, 103718.

(7) Asrat, F. S.; Ghebrab, T. T. Effect of Mill-Rejected Granular Cement Grains on Healing Concrete Cracks. *Materials* **2020**, *13*, 840.

(8) Fernandez, C. A.; Correa, M.; Nguyen, M. T.; Rod, K. A. Progress and challenges in self-healing cementitious materials. *J. Mater. Sci.* **2021**, *56*, 201−230.

(9) Wang, X. F.; Yang, Z. H.; Fang, C.; Han, N. X.; Zhu, G. M.; Tang, J. N.; Xing, F. Evaluation of the mechanical performance recovery of self-healing cementitious materials - its methods and future development: A review. *Constr. Build. Mater.* **2019**, *212*, 400−421.

(10) Chang, T.; Panhwar, F.; Zhao, G. Flourishing Self-Healing Surface Materials: Recent Progresses and Challenges. *Adv. Mater. Interfaces* **2020**, *7*, 1901959.

(11) Han, T.; Wang, X.; Li, D.; Li, D.; Han, N. Influence of strain rate on mechanical characteristic and pore structure of self-healing cementitious composites with epoxy/urea-formaldehyde microcapsules. *Constr. Build. Mater.* **2021**, *268*, 121138.

(12) Han, T.; Xing, F.; Han, N.; Li, D. Stress and strain behavior of cementitious composites with epoxy/urea-formaldehyde microcapsules under uniaxial tests. *J. Ceram. Process. Res.* **2019**, *20*, 46−55.

(13) Nguyen, T. H.; Ghorbel, E.; Fares, H.; Cousture, A. Bacterial self-healing of concrete and durability assessment. *Cem. Concr. Compos.* **2019**, *104*, 103340.

(14) Jeong, B.; Jho, E. H.; Kim, S. H.; Nam, K. Effect of Calcium Organic Additives on the Self-Healing of Concrete Microcracks in the Presence of a New Isolate Bacillus sp. BY1. *J. Mater. Civ. Eng.* **2019**, *31*, 04019227.

(15) Srinivassarame, L. Studies on Self-healing Sustainable Concrete Using Bacterial Carbonate Precipitate. *Int. J. Appl. Eng. Res.* **2020**, *13*, 16719−16728.

(16) Khushnood, R. A.; ud din, S.; Shaheen, N.; Ahmad, S.; Zarrar, F. Bio-inspired self-healing cementitious mortar using Bacillus subtilis immobilized on nano-/micro-additives. *J. Intell. Mater. Syst. Struct.* **2019**, *30*, 3−15.

(17) Hamza, O.; Esaker, M.; Elliott, D.; Souid, A. The effect of soil incubation on bio self-healing of cementitious mortar. *Mater. Today* **2020**, *24*, 100988.

(18) Xu, H.; Lian, J.; Gao, M.; Fu, D.; Yan, Y. Self-Healing Concrete Using Rubber Particles to Immobilize Bacterial Spores. *Materials* **2019**, *12*, 2313.

(19) Jiang, L.; Jia, G.; Jiang, C.; Li, Z. Sugar-coated expanded perlite as a bacterial carrier for crack-healing concrete applications. *Constr. Build. Mater.* **2020**, *232*, 117222.

(20) Minto, J. M.; Lunn, R. J.; El Mountassir, G. Development of a Reactive Transport Model for Field-Scale Simulation of Microbially Induced Carbonate Precipitation. *Water Resour. Res.* **2019**, *55*, 7229−7245.

(21) Chae, S. H.; Chung, H.; Nam, K. Evaluation of microbially Induced calcite precipitation (MICP) methods on different soil types for wind erosion control. *Environ. Eng. Res.* **2020**, *26*, 123−128.

(22) Jeong, J.-H.; Jo, Y.-S.; Park, C.-S.; Kang, C.-H.; So, J.-S. Biocementation of Concrete Pavements Using Microbially Induced Calcite Precipitation. *J. Microbiol. Biotechnol.* **2017**, *27*, 1331−1335.

(23) Jiang, L.; Jia, G.; Wang, Y.; Li, Z. Optimization of Sporulation and Germination Conditions of Functional Bacteria for Concrete Crack-Healing and Evaluation of their Repair Capacity. *ACS Appl. Mater. Interfaces* **2020**, *12*, 10938−10948.

(24) Souza, L.; Al-Tabbaa, A. Microfluidic fabrication of microcapsules tailored for self-healing in cementitious materials. *Constr. Build. Mater.* **2018**, *184*, 713−722.

(25) Wang, J. Y.; Snoeck, D.; Van Vlierberghe, S.; Verstraete, W.; De Belie, N. Application of hydrogel encapsulated carbonate precipitating bacteria for approaching a realistic self-healing in concrete. *Constr. Build. Mater.* **2014**, *68*, 110−119.

(26) Liu, C.; Xu, X.; Lv, Z.; Xing, L. Self-healing of Concrete Cracks by Immobilizing Microorganisms in Recycled Aggregate. *J. Adv. Concr. Technol.* **2020**, *18*, 168−178.

(27) Xu, J.; Tang, Y.; Wang, X.; Wang, Z.; Yao, W. Application of ureolysis-based microbial CaCO3 precipitation in self-healing of concrete and inhibition of reinforcement corrosion. *Constr. Build. Mater.* **2020**, *265*, 120364.

(28) Zheng, T.; Su, Y.; Zhang, X.; Zhou, H.; Qian, C. Effect and Mechanism of Encapsulation-Based Spores on Self-Healing Concrete at Different Curing Ages. *ACS Appl. Mater. Interfaces* **2020**, *12*, 52415−52432.

(29) Vijay, K.; Murmu, M. Effect of calcium lactate on compressive strength and self-healing of cracks in microbial concrete. *Front. Struct. Civ. Eng.* **2019**, *13*, 515−525.
(30) Zhou, Y.; Sheng, Q.; Li, N.; Fu, X.; Zhang, Z.; Gao, L. A Constitutive Model for Rock Materials Subjected to Triaxial Cyclic Compression. *Mech. Mater.* **2020**, *144*, 103341.
(31) Liu, C.; Xing, L.; Liu, H.; Huang, W.; Nong, X.; Xu, X. Experimental on repair performance and complete stress-strain curve of self-healing recycled concrete under uniaxial loading. *Constr. Build. Mater.* **2021**, *285*, 122900.
(32) Ding, X.; Li, C.; Li, Y.; Lu, Y.; Song, C.; Zhao, S. Experimental and numerical study on stress-strain behavior of self-compacting SFRC under uniaxial compression. *Constr. Build. Mater.* **2018**, *185*, 30−38.
(33) Wang, L.; Gao, P.; Tian, Y.; Yao, C.; Hao, D.; Wang, Z. Experimental Study on Axial Tensile Stress-Strain Relationship of High Crack Resistance Concrete. *IOP Conf. Ser.: Earth Environ. Sci.* **2021**, *719*, 022025.

https://doi.org/10.1021/acsomega.1c05971
ACS Omega 2022, 7, 2947−2959